SolarPACES 2024, 30th International Conference on Concentrating Solar Power, Thermal, and Chemical Energy Systems

Analysis and Simulation of CSP and Hybridized Systems

https://doi.org/10.52825/solarpaces.v3i.2468

Published: 28 Aug. 2025

Multi-Flow Falling Particle Receiver Modeling

Ahmed Mohamed[1,*], Gowtham Mohan[2], Peter Vorobieff[1], and Nathan Schroeder[3]

[1]University of New Mexico, Albuquerque, NM, United States of America

[2]University of Houston, Houston, TX, United States of America

[3]Sandia National Labs, Albuquerque, NM, United States of America

*Correspondence: Ahmed Mohamed, ahmedmuhamed@unm.edu

Abstract. Generation 3 Concentrating Solar Power systems use solid particles for heat transfer and thermal energy storage. Particle-based systems use a falling particle receiver with an open cavity where particles flow together as a curtain that is directly exposed to solar radiation absorbed by the particles as they descend. The efficiency of the receiver depends on curtain opacity (influenced by the particle mass flow rate), the average particle temperature, and environmental factors. We present a free-falling particle receiver design that incorporates ten individually controlled valves for precise particle supply management. Each valve is equipped with a slide gate and an actuator, ensuring a consistent mass flow rate. In a uniform mass flow rate curtain, the hottest particles accumulate in the center due to non-uniform flux distribution, leading to higher radiative and advective losses. Accordingly, lower flux levels at the periphery result in lower temperature particles. Our modular valve design enhances receiver efficiency by improving curtain opacity in key areas. The outer valves have the lowest mass flow rate, while the center valves have the highest, allowing more uniform heating. The 10-section model outperforms the 1D model by reaching a maximum efficiency of 85%, compared to 84%.

Keywords: CSP, 2D Model, Benchmark, EES, Particle Receiver

1. Introduction

Concentrated Solar Power (CSP) has gained attention as a reliable source of baseline renewable energy. Research in the US supports the Department of Energy's goal to reduce the Levelized Cost of Electricity (LCOE) to $0.05/kWh [1], [2], which requires high thermal efficiencies. The CSP Plant model presented in this study uses supercritical CO_2 (sCO_2) power cycles, recommended by the National Renewable Energy Laboratory roadmap [1], [3]. These systems require peak central receiver temperatures above 750°C. The DOE down-selected the solid particle heat transfer and thermal storage medium as it is most likely to achieve the 0.05 $/kWh target. Performance and characteristics of the free-falling particle receiver were simulated numerically [4], [5], [6], [7]. Our earlier work features a receiver model [7] created to replicate the essential physical phenomena in a falling particle receiver (FPR) for CSP. The one-dimensional (1D) CFD model validated with on-sun test data [8] incorporates assumptions and simplifications, such as treating the curtain area the same as the receiver area. It gathered parameters from literature and optimized others, including curtain thickness, particle volume fraction, and radiative properties, to match CFD model predictions. The Monte Carlo Ray-Tracing model was used to evaluate optical properties of the curtain's absorbance, transmittance, and reflectance [9]. The model, validated against CFD simulations, accurately predicted receiver performance. Design optimization focused on heat transfer and absorbance [9], [10]. The 1D model

implemented in EES (Engineering Equation Solver) software considers energy, mass, and momentum balance equations in discretized sections of the particle curtain. These equations calculate the particle outlet and receiver back wall temperatures based on the incident flux [7]. Now we introduce a two-dimensional (2D) model that builds upon earlier 1D work [7], with an additional dimension that accounts for the width of the particle curtain. This approach pursues two main objectives: improving modeling efficiency and optimizing mass flow rate to enhance thermal efficiency for a new receiver design with a modular particle curtain valve developed to address nonuniform heating caused by the flux distribution on the receiver. This design also aims to improve valve serviceability. By optimizing mass flow in each section, curtain opacity and thermal efficiency are increased. Reduced flux on the sides lowers mass flow there, allowing side particles to absorb more heat and capture more solar radiation. We compare the one-dimensional and two-dimensional models, focusing on the optimization of mass flow within each curtain section and the maximum turn down ratio of the FPR. This model will be implemented in future work where a particle-based techno-economic model is utilized to assess the design effects on performance, levelized cost of electricity, and receiver outlet temperature.

2. Model

Previous research led to a 1D FPR model describing the performance of a receiver with a single valve, uniform heat flux, and mass flow rate. The new 2D model simulates the receiver performance by discretizing the analysis over two dimensions: the falling direction *x* and the curtain width direction *y*. The curtain is divided into 40 discrete segments along the *y*-axis, while the *x*-direction is discretized by the desired number of control sections. A 2D model with 3 sections is shown in *Figure 1***.** The *y*-direction discretization accounts for the variability of solar radiation, particle curtain transmissivity, and heat losses in the falling direction. Discretizing the *x* direction enables each curtain section to vary its mass flow independently. The 1D model was designed to determine the outlet temperature of the curtain, the back wall temperature, and the thermal efficiency of the receiver [7]. The 2D model adds curtain width for better evaluation of the effect of the mass flow rate on thermal efficiency. Back wall temperature and efficiency are calculated with fixed particle inlet and solar input to optimize mass flow. The 2D model uses the same approach as the 1D model but with updated inputs, assumptions, and boundary conditions. Code adjustments were made for the 10-section setup.

2.1 Model structure and assumptions

The following assumptions are considered in the 2D code according to the conservation equations and the boundary conditions:

Solar radiation is perpendicular to the curtain.

No interaction between the falling particles in the y direction and the x direction [11], [12].

Each section of the curtain will receive a designated amount of flux, determined by an actual flux distribution.

The flux value assigned to each section accurately represents the average heat flux applied across the entire area of that section, guaranteeing that every section receives a consistent and averaged value of heat flux. This approach results in a heat flux distribution that closely mirrors the actual flux distribution experienced by the receiver.

The primary physical phenomena in a particle receiver are predominantly observed in the direction of descent, indicating that changes in parameters like volume fraction and particle curtain thickness primarily occur along the y-axis.

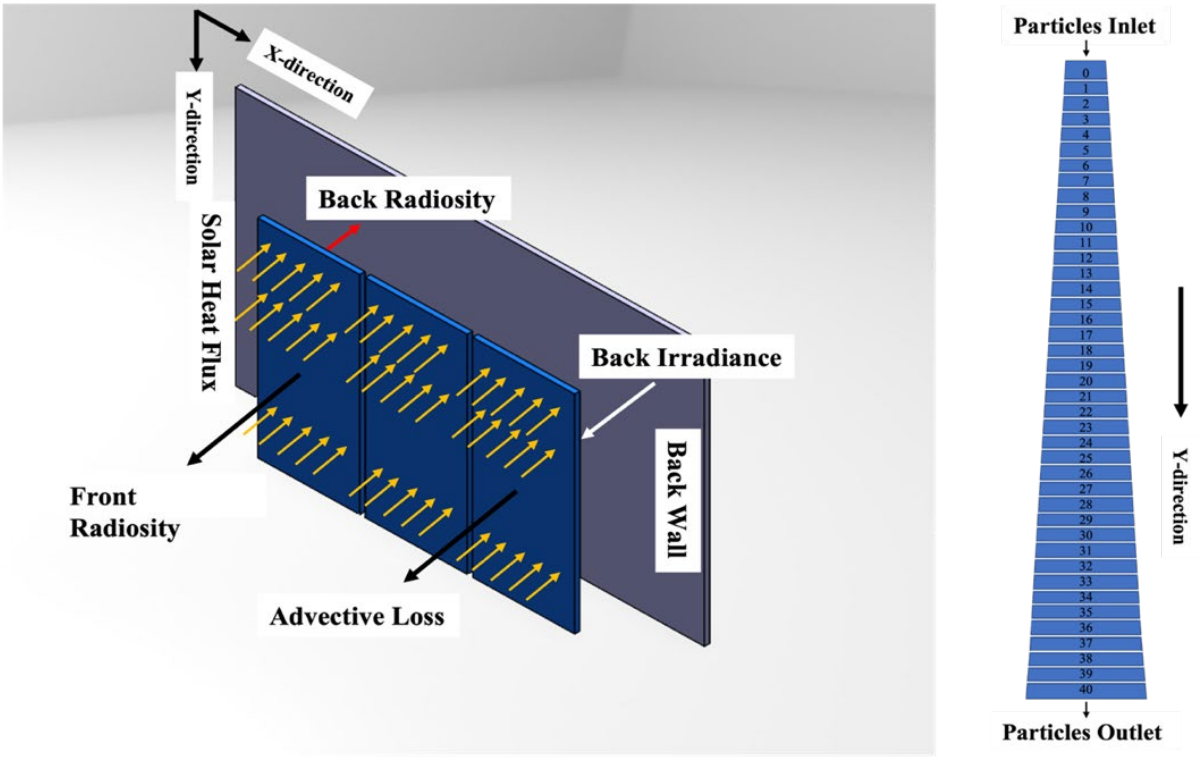

Figure 1. *(**a**) Simplified diagram of the 2D free-falling particle receiver heat exchange model with 3 sections. (**b**) Y-direction discretization.*

The conservation equations used in this model are Eq. (1) - mass balance, Eq. (2) - momentum balance, and Eq. (3) - energy balance.

$$-\frac{d(\varphi_P(x,y)th_c(x,y)\rho_P v_P(x,y))}{dy}=0 \tag{1}$$

$$-\frac{d(\varphi_P d\varphi_P(x,y)th_c(x,y)\rho_P v^2{}_P(x,y))}{dy}+\varphi_P(x,y)th_c(x,y)\rho_P g=0 \tag{2}$$

$$-\frac{d(\varphi_P d\varphi_P(x,y)th_c(x,y)\rho_P v_P(x,y)h_P(x,y))}{dy}+g_{c,_{front}}(x,y)-j_{c,_{front}}(x,y)+g_{c,_{back}}(x,y)-j_{c,_{back}}(x,y)-q''_{adv}(x,y)=0 \tag{3}$$

Here φ_P is particle volume fraction, th_c the curtain thickness (m), ρ_P the particle density $(\mathrm{kg/m^3})$, v_P the velocity $(\mathrm{m/s})$, h_P the particle enthalpy $(\mathrm{J/kg})$, g_c the irradiances $(\mathrm{W/m^2})$, j_c the radiosities which are the sum of the outgoing energy from a surface $(\mathrm{W/m^2})$, and q''_{adv} the advection thermal loss $(\mathrm{W/m^2})$. The equations in the code are primarily presented in differential form, with EES solving them for each segment to determine the thermal efficiency of the receiver, as well as the velocity and outlet temperature. As each section may operate with a distinct mass flow rate, the thickness was calculated depending on the input mass flow rate of each section.

$$\eta_{reciver}=\frac{\Delta h_p \dot{m}}{q''_{solar}} \tag{4}$$

The convection coefficient was calculated by the function $htc_{estimation}$ which takes T_{in}(℃), T_{out}(℃), T_{air}(℃), and H(m). T_{in}being the particle inlet temperature, T_{out} is the outlet particle temperature, T_{air} is the ambient air temperature, and H is the height of the curtain. The advection heat transfer coefficient is determined by employing a conventional Nusselt number formulation, analogous to the methodology utilized for forced convection heat transfer coefficients.

$$Nu = \mathrm{A} + \mathrm{B} \cdot \mathrm{Re}^{\mathrm{c}} \tag{5}$$

$$v_P = \sqrt{2gH} \tag{6}$$

$$Re = v_P H \frac{\rho_{air,Nu}}{\mu_{air,Nu}} \tag{7}$$

Constants *A*, *B*, and *C* were determined by fitting the 1D model to match the results of the CFD model. *H* represents the height, and *g* - gravity. *Re* is the Reynolds calculated with the curtain height as the characteristic length and the velocity v_P of the particles. Air properties are density $\rho_{air,Nu}$ and viscosity $\mu_{air,Nu}$. The convection coefficient is used as an initial condition in the energy balance equation and in the calculation of convection losses as shown in Eq. (4):

$$q''_{conv}(x,y) = \left(\frac{1}{\mathrm{htc_{cv,w}}} + \frac{th_w}{K_w}\right)^{-1} (T_w(x,y) - T_{\mathrm{o}}) \tag{8}$$

For $q''_{conv}(\mathrm{W/m^2})$, $\mathrm{htc_{cv,w}}$ is back wall, heat transfer convective coefficient, $K_w(\mathrm{W/m \cdot K})$ is the back wall conductivity, $T_w(x,y)$ (℃)is the back wall temperature, $th_w(m)$ is back wall thickness, and T_{o}(℃) is the ambient temperature. The irradiances and the radiosities are calculated using the equations from the 1D model [7]. These equations were modified to suit the 2D model, however, the analytical calculations were kept. Optical properties, namely reflectance and transmittance, were calculated following an analytical model [13].

2.2 Parameters

This section outlines the main parameters used in the 2D code, including both input and assumed values. The input parameter utilized in the code is shown in *able 1*. Some of the parameters were extracted from Ref. [7], while the rest of the parameters were either referenced from previous work or assumed [7], [14], [15], [16], [17]. The parameters denoted with an asterisk (*) represent variables that possess an array of values. This indicates that these parameters must be input individually for each section. The model relies on thickness th_c (m), convection coefficient, particle enthalpy h_p (J/Kg), particle volume fraction φ_P, and temperature (℃), the initial velocity v_P (m/s), convection coefficient, and particle enthalpy as inputs, which are determined before the conservation equations are applied [7]. The initial section curtain thickness can be evaluated by the following equations (mass balance equation)

$$\varphi_P . th_c . \rho_P . w_c . v_P = \dot{m} \tag{9}$$

Table 1. *Input parameters for the 2D model*

Parameter	Value	Reference
Curtain height	5.6 m	Assumed
Aperture aspect ratio, AR	1	Assumed
Number of sections	3	Assumed
Back wall emissivity, ε_w	0.8	[7]
*Solar radiation, q''_{solar}	Figure 2	
Back wall thickness, th_w	0.05 m	[7]
Ambient temperature, T_o	20 °C	[7]
Back wall conductivity, K_w	0.2 W/(m K)	[7]
Back wall heat transfer coefficient, $htc_{cv,w}$	10 W/(m2K)	[7]
Particle diameter, d_p	350 μm	[15]
Particle specific heat capacity, C_p	1.2 kJ/(kg K)	[14]
Particle conductivity, k_p	2 W/(m K)	[14]
Particle density, ρ_p	3550 kg/m^3	[14]
Particle absorptivity, α_p	0.9	[13]
Curtain width	5.6 m	Assumed
Curtain emittance, ε_c	0.9	[11]
*Particle inlet temperature, T_{in}	200 °C - 400 °C	Assumed
Mass flow rate, $\dot{m}$	To be analyzed	
Aperture area, A_{ap}	31.36 m^2	Assumed
Inlet particle volume fraction, φ_p	0.6	[16]

Equations 4-6 use boundary conditions to calculate the initial thickness of the section, where the mass flow rates in the three sections are $\dot{m}_1$, $\dot{m}_2$, and $\dot{m}_3$ respectively. In the 1D model [7], the heat flux was assumed as uniform across the entire curtain. However, the actual heat flux distribution over the curtain is not uniform as shown in *Figure 2*. The heat flux is mainly concentrated at the center, forming a hotspot, and decreases progressively toward the corners.

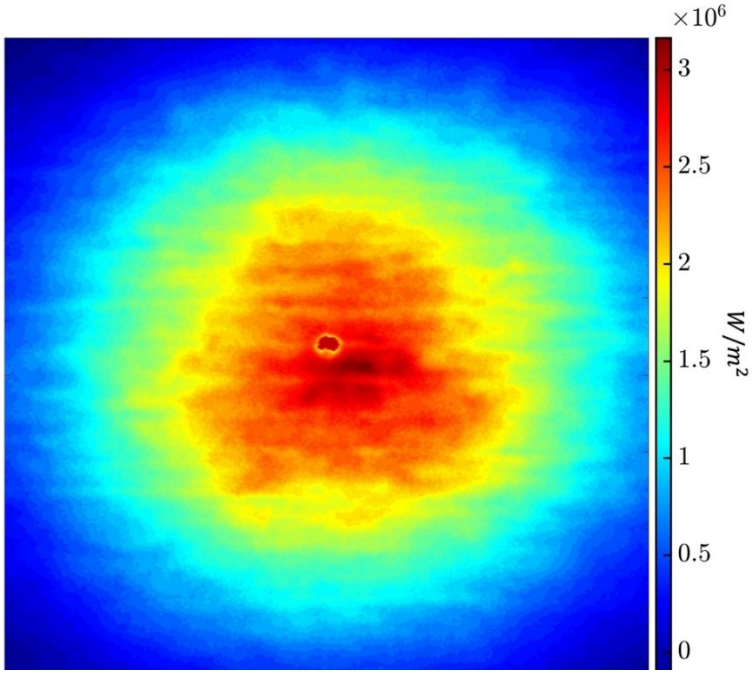

Figure 2. *Diagram of 2D falling particle receiver heat flux distribution over the curtain. Units on the left axis are meters.*

3. Results and discussion

The initial phase of testing the two-dimensional model involved the verification of the solution to ensure the accuracy of the algorithm implemented within the code. When the same inputs were used in the 1D and the 2D models, the results agreed perfectly with each other, with a 100% match. Traditionally, falling particle receivers use a single valve with a slide gate and actuator to ensure a consistent mass flow rate across the curtain. With an uneven flux profile, this design produces a high-temperature zone at the center, increasing radiative and convective losses. By controlling individual curtain sections, the particle temperature at the center can be reduced by increasing the mass flow rate, while maintaining the receiver's outlet temperature. Simultaneously, lowering the mass flow rate at the corners enhances heat absorption and overall efficiency. The optimization of the mass flow rate will lead to a reduction in radiative losses, enhancing the overall thermal efficiency of the receiver. The code was executed utilizing the midday heat flux distribution, along with the specified input parameters and initial conditions for both the single-section and 10-section models. The heat flux for midday is 0.98 MW/m^2. The input temperature ranged from 400°C to 600°C, ideal for sCO_2 Brayton, Air Brayton, and Steam Rankine cycles. The graphs with the output of the code, thermal efficiency, and outlet temperature are shown in *Figure 3.*

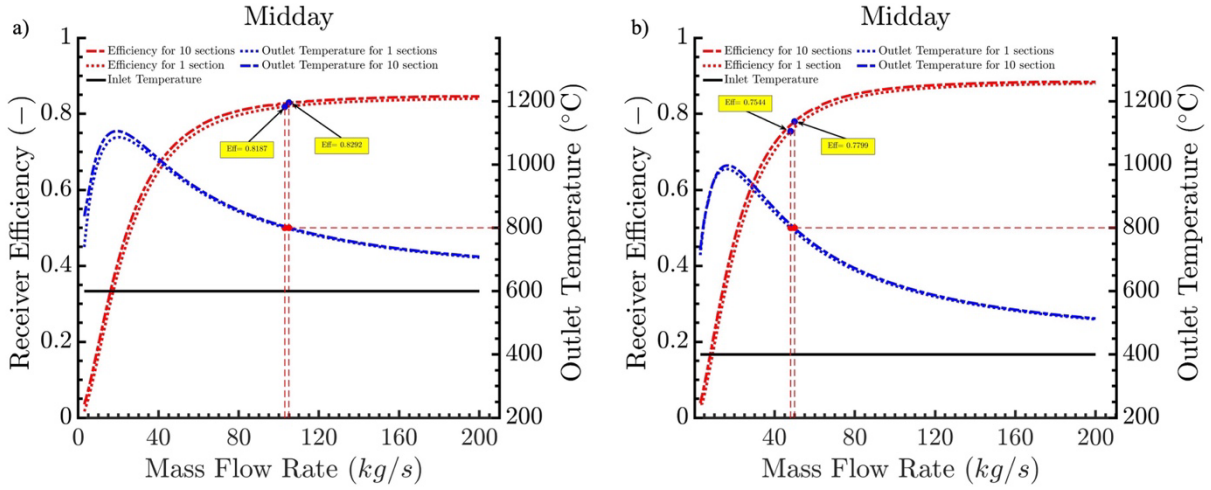

Figure 3. *(**a**) Receiver thermal efficiency vs. mass flow rate and outlet temperature under midday flux distribution, with an inlet temperature 400°C. (**b**) Receiver thermal efficiency vs. mass flow rate and outlet temperature for midday flux distribution, input temperature 600°C*

In *Figure 3*(a), the 10-section receiver model shows improved performance over the 1D model, reaching a maximum efficiency of 85%, exceeding the 84% efficiency attained by the 1D model. The output temperature has exhibited a similar trend, albeit with a slight variation. As mentioned earlier, for the sCO_2 Brayton cycle, an inlet temperature of 600 °C, combined with a target temperature differential of 200 °C, yields an outlet temperature of 800 °C. The thermal efficiency at 800 °C was particularly highlighted, as this temperature represents a crucial focal point in the analysis. In Fi*gure 3*(b), the ten-section model demonstrated higher thermal efficiency, attaining a maximum value of 88.7%, in contrast to the one-section model, which achieved a maximum efficiency of 88.03%. The inlet temperature is set at 600 °C to maximize the efficiency of the Air Brayton and Steam Rankine cycles, ensuring a stable outlet temperature of 800 °C. The efficiency highlighted in yellow was used to validate both the model and its results as the 1D model has been validated by comparing it to CFD models[7]. The difference in efficiency between the two models can be utilized to determine the corresponding difference in mass flow rate, as indicated between the two dashed lines. This is accomplished by multiplying the efficiency difference by the power input and then dividing the result by the specific heat capacity C_p and the temperature differential. The second case assesses the receiver's performance during early-day flux conditions, utilizing an input flux of 0.65 MW/m².

The results obtained for this early-day flux scenario were derived utilizing the same methodology that was employed in the analysis of the midday flux condition.

The early-day study showed that the 10-section model consistently outperformed the 1-section model. At an input temperature of 600 °C, the 10-section model achieved a maximum efficiency of 79.5%, compared to 78% for the 1-section model. At 400 °C input, the 10-section model reached 85% efficiency, slightly higher than the 1-section model's 84%. As previously noted, achieving an outlet temperature of 800 °C is crucial for desired efficiency, and the study confirmed that the 1-section model was unable to reach this target, unlike the 10-section model. This discrepancy prompts us to consider the minimum heat flux or power input necessary to achieve the intended temperature difference in the model. An additional evaluation was subsequently conducted to assess the turn down ratio, aiming to ascertain the minimum power input necessary to attain the desired temperature differential for both models. The turn down ratio is defined as the rated power divided by the minimum power. This set of graphs is presented in *Figure 4.*

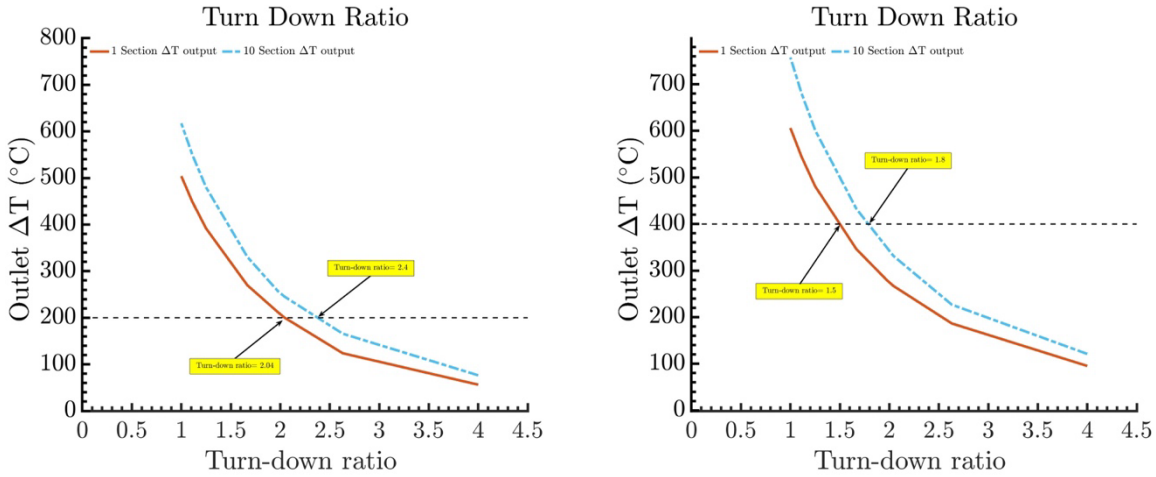

Figure 4. *(**a**) turn down ratio for dt 200 (**b**) turn down ratio for dt 400*

The 10-section model attains the requisite temperature difference with a diminished power input, signifying that the power necessary to achieve a specific level of efficiency has been reduced in comparison to the 1D model. This highlights the significant advantage of the 10-section model; it consistently delivers the desired outcomes, even during specific times of the day when the 1D model fails to generate the necessary performance. The 10-section model, aimed at maximizing mass flow rate, significantly outperformed the 1D model during midday and early conditions when subjected to heat flux inputs of 0.98 MW/m² and 0.65 MW/m², respectively. This multi-flow particle receiver design not only enhanced the receiver's overall performance throughout the day but also functioned more efficiently with lower power inputs. The notable improvement can be linked to the optimization of the mass flow rate. This strategy enhances particle absorbance of solar radiation by lowering mass flow rates at the periphery, while simultaneously increasing mass flow rates in the center to minimize radiative losses.

4. Conclusion

This study introduced a 10-section model for a free-falling particle receiver with a multi-valve design created to reduce the impact of solar flux on the curtain and improve the thermal efficiency of the receiver by optimizing mass flow rates. Our code offers excellent adaptability, allowing for modifications to the number of sections as needed. This adaptability opens new avenues for future research to explore how varying the number of sections affects system performance. Our study examined the 10-section and 1-section receiver models under various conditions, highlighting the advantages of the 10-section model. Remarkably, the 10-section model consistently demonstrated superior performance. The 10-section model showed great

thermal efficiency, reaching 79.5% at 600 °C and 85% at 400 °C. This performance outstrips that of the 1-section model in both scenarios. This achievement was possible by optimizing the mass flow rate through the ten valves, which were designed to match the heat flux distribution. This tailored approach significantly enhanced both the opacity and absorptance of the particle curtain. The focused optimization of mass flow rate has notably increased efficiency, particularly in light of the precise flux distribution. The findings show that the 2D model matches the results of the 1D model, confirming the 2D model's reliability. The results highlight the vital importance of receiver design in attaining the target outlet temperature of 800°C, which is crucial for maximizing efficiency in concentrated solar power applications. The success of the 10-section model raises important questions about the minimum heat flux or power needed for better performance in simpler receiver designs, especially since the 1-section model didn't reach the same temperature. These findings suggest that the 2D model provides considerable performance advantages. It is especially beneficial in applications demanding high efficiency and effectiveness. The 2D model excels in high thermal efficiency and precise temperature control. Future research should focus on optimizing heat flux and power input to streamline receiver designs. It shows adaptability to various inputs like solar flux and mass flow, allowing detailed analysis of thermal efficiency. The model additionally should take into account elements such as the effects of wind and the interactions between particles. The 2D model will be utilized in a particle-based techno-economic analysis to evaluate the impact of the receiver's innovative design on plant performance, the levelized cost of electricity, and the thermal cycling of the receiver's back wall material.

Data availability statement

The data for this research work can be accessed directly from the authors.

Underlying and related material

Related materials can be obtained directly from the authors.

Author contributions

The conceptualization, development of materials, methodology, experimental procedures, and analysis of results presented in this paper were conducted under the supervision and guidance of Professors Peter Vorobieff, Gowtham Mohan, and Engineer Nathan Schroeder.

Competing interests

The authors declare no competing interests.

Funding

This research is supported by the Sandia National Laboratories via Standard Purchase Order 2469980.

Acknowledgement

This work was conducted at the University of New Mexico, a public research institution supported by the State of New Mexico. Research was carried out within the Department of Mechanical Engineering, with support from institutional and federal research initiatives.

References

[1] M. Mehos *et al.*, "Concentrating Solar Power Gen3 Demonstration Roadmap," NREL/TP--5500-67464, 1338899, Jan. 2017. doi: 10.2172/1338899.

[2] B. H. Mills, C. K. Ho, N. R. Schroeder, R. Shaeffer, H. F. Laubscher, and K. J. Albrecht, "Design Evaluation of a Next-Generation High-Temperature Particle Receiver for Concentrating Solar Thermal Applications," *Energies*, vol. 15, no. 5, p. 1657, Feb. 2022, doi: 10.3390/en15051657.

[3] University of Adelaide *et al.*, "Gen 3 Particle Pilot Plant (G3P3) -- High-Temperature Particle System for Concentrating Solar Power (Phases 1 and 2)," SAND2021-14614, 1832285, 701739, Nov. 2021. doi: 10.2172/1832285.

[4] A. S. Oles and G. S. Jackson, "Modeling of a concentrated-solar, falling-particle receiver for ceria reduction," *Solar Energy*, vol. 122, pp. 126–147, Dec. 2015, doi: 10.1016/j.solener.2015.08.009.

[5] J. Hruby, R. Steeper, G. Evans, and C. Crowe, "An Experimental and Numerical Study of Flow and Convective Heat Transfer in a Freely Falling Curtain of Particles," *Journal of Fluids Engineering*, vol. 110, no. 2, pp. 172–181, Jun. 1988, doi: 10.1115/1.3243531.

[6] M. Röger, L. Amsbeck, B. Gobereit, and R. Buck, "Face-Down Solid Particle Receiver Using Recirculation," *Journal of Solar Energy Engineering*, vol. 133, no. 3, p. 031009, Aug. 2011, doi: 10.1115/1.4004269.

[7] L. F. González-Portillo, V. Soria-Alcaide, K. Albrecht, C. K. Ho, and B. Mills, "Benchmark and analysis of a particle receiver 1D model," *Solar Energy*, vol. 255, pp. 301–313, May 2023, doi: 10.1016/j.solener.2023.03.046.

[8] B. Mills, S. Lee, K. Albrecht, and C. Ho, "Thermal Performance of Commercial Falling Particle Receivers at Different Scales.," Sandia National Lab.(SNL-NM), Albuquerque, NM (United States), 2022. Accessed: Apr. 07, 2025. [Online]. Available: https://www.osti.gov/servlets/purl/2003941

[9] L. F. González-Portillo, R. Abbas, K. Albrecht, and C. Ho, "Analysis of optical properties in particle curtains," *Solar Energy*, vol. 213, pp. 211–224, Jan. 2021, doi: 10.1016/j.solener.2020.11.012.

[10] A. Kumar, W. Lipiński, and J.-S. Kim, "Numerical modelling of radiation absorption in a novel multi-stage free-falling particle receiver," *International Journal of Heat and Mass Transfer*, vol. 146, p. 118821, Jan. 2020, doi: 10.1016/j.ijheatmasstransfer.2019.118821.

[11] A. Kumar, J.-S. Kim, and W. Lipiński, "Radiation Absorption in a Particle Curtain Exposed to Direct High-Flux Solar Irradiation," *Journal of Solar Energy Engineering*, vol. 140, no. 6, p. 061007, Dec. 2018, doi: 10.1115/1.4040290.

[12] M. S. Rahman, A. Mohamed, A. Sweis, J. Chavez, and P. Vorobieff, "Development of a novel method to characterize shock waves interaction with solid objects," *Sci Rep*, vol. 14, no. 1, p. 28956, Nov. 2024, doi: 10.1038/s41598-024-79220-6.

[13] B. E. Romero, J. M. Reisner, P. Vorobieff, and S. V. Poroseva, "Statistical characterization of a shock interacting with an inclined gas column," *J. Fluid Mech.*, vol. 971, p. A26, Sep. 2023, doi: 10.1017/jfm.2023.660.

[14] C. K. Ho, B. Mills, and J. M. Christian, "Volumetric Particle Receivers for Increased Light Trapping and Heating," in *Volume 1: Biofuels, Hydrogen, Syngas, and Alternate Fuels; CHP and Hybrid Power and Energy Systems; Concentrating Solar Power; Energy Storage; Environmental, Economic, and Policy Considerations of Advanced Energy Systems; Geothermal, Ocean, and Emerging Energy Technologies; Photovoltaics; Posters; Solar Chemistry; Sustainable Building Energy Systems; Sustainable Infrastructure and Transportation; Thermodynamic Analysis of Energy Systems; Wind Energy Systems and Technologies*, Charlotte, North Carolina, USA: American Society of Mechanical Engineers, Jun. 2016, p. V001T04A016. doi: 10.1115/ES2016-59544.

[15] B. Mills, R. Shaeffer, C. K. Ho, and L. Yue, "Modeling the Thermal Performance of Falling Particle Receivers Subject to External Wind," in *ASME 2019 13th International Conference on Energy Sustainability*, Bellevue, Washington, USA: American Society of Mechanical Engineers, Jul. 2019, p. V001T03A011. doi: 10.1115/ES2019-3913.

[16] C. K. Ho *et al.*, “Characterization of Particle Flow in a Free-Falling Solar Particle Receiver,” *Journal of Solar Energy Engineering*, vol. 139, no. 2, p. 021011, Apr. 2017, doi: 10.1115/1.4035258.

[17] B. Gobereit, L. Amsbeck, R. Buck, R. Pitz-Paal, M. Röger, and H. Müller-Steinhagen, “Assessment of a falling solid particle receiver with numerical simulation,” *Solar Energy*, vol. 115, pp. 505–517, May 2015, doi: 10.1016/j.solener.2015.03.013.